ACS EARTH AND SPACE CHEMISTRY

http://pubs.acs.org/journal/aesccq

Article

Helium Isotopic Signature of a Plate Boundary Suture in an Active Arc−Continent Collision

Ai-Ti Chen, Yuji Sano, Timothy B. Byrne,* Naoto Takahata, Tsanyao Frank Yang, Yunshuen Wang, and Chuan-Chou Shen*

Cite This: *ACS Earth Space Chem.* 2020, 4, 1237−1246

Read Online

ACCESS | Metrics & More | Article Recommendations

ABSTRACT: We report new noble gas signatures of groundwaters, hot springs, and bedrock samples from two major fault systems that form the plate boundary suture between the Eurasian Plate and the Philippines Sea Plate. In the south, the Eurasian Plate dips east beneath the Philippine Sea Plate, and the boundary between the arc and accretionary prism is marked by the Chihshang Fault, which also dips east beneath the arc. The fault is well-defined by seismicity and extends to at least 25 km, close to the crust−mantle boundary. This fault could be an important conduit for the passage of mantle helium along the suture. In the north, as the subduction direction flips from the east-dipping Eurasian Plate to the north-dipping Philippine Sea Plate, the plate boundary fault is represented by a more complex system of east- and west-dipping structures. Low helium isotopes in this area evidence the weaker mantle signal, both before and after a M_w 6.4 earthquake. It is possible that as the subduction direction flips from south to north along strike, the tortuosity of the fault-related conduits increases, reducing the flow and limiting the release of mantle-derived gases.

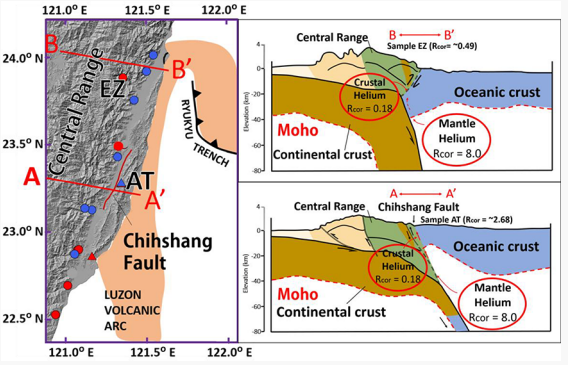

KEYWORDS: *noble gases, plate boundary suture, subduction polarity reversal, Hualien earthquake*

1. INTRODUCTION

Active arc−continental collisions are one type of convergent margin where the subduction of oceanic lithosphere and consequent welding of continental masses result in a suture zone marked, in part, by fragments of the missing ocean.[1] The involvement of buoyant continental crust, which resists subduction, can also lead to the cessation of subduction along the suture and formation of a new subduction zone, often with the opposite polarity or dip direction (e.g., Chemenda et al.).[2] Fault zones generated along the suture and associated with a reversal in subduction polarity can provide conduits for the transfer of heat and fluids from deep within the collision.[3−5] For example, fluids may tap mantle sources and be characterized by geochemical fingerprints, such as noble gases.[6] Isotopic signatures of noble gases can be used as natural tracers for tracking the fluid migration process at crustal scales with the important advantage that mantle, crustal, and atmospheric sources are characterized by unique isotopic signatures of helium ($^3He/^4He$) and neon−helium ratios ($^{20}Ne/^{22}Ne$).[7−10] These ratios, integrated with geophysical data, can offer clues on the processes controlling regional-scale fluid transfer in zones of continental collision, where both mantle and crustal sources can be important. Noble gas investigation in suture zones can reveal important information about both shallow (e.g. the Pyrenees; the Urals) and deep structures (e.g. the Yarlung-Zangbo suture; Japan; Italy).[4,11−18] For example, the source of ^3He close to the Yarlung-Zangbo suture is likely either asthenosphere accessed by faults and shear zones that cut through subducting Indian lithospheric mantle or incipient melt of the Asian lithospheric mantle at the Moho north of the northern edge of underthrust India (the "mantle suture") which must therefore lie close to the Yarlung-Zangbo suture.[14] This fluid transfer may also be influenced by earthquakes, where changes in volumetric strain drive fluid migration and affect the helium isotope ratios (e.g. Buttitta et al.;[19] Sano et al.[20]).

The Taiwan orogenic system, with shallow (<10 km depth) and deep tectonic structures (>10 km, down to Moho depths), is situated in an active arc−continent collision zone[21−27] and serves as a natural laboratory for evaluating the flow patterns of mantle-derived fluids along the plate boundary suture zone.

Received: February 6, 2020
Revised: June 25, 2020
Accepted: July 15, 2020
Published: July 15, 2020

Chen et al. suggested that fluids collected along the trace of a major fault zone west of the suture most likely originated from the mantle of the Eurasian Plate and migrated along a crustal-scale fault system.[8] However, along the suture zone, which is marked by the longitudinal valley (LV), few direct geochemical records exist, which limits our understanding of the involvement of interconnected fluids from the upper mantle. To further clarify the regional character of this arc−continent collision system, we investigated the LV (Figure 1b), including the active Chihshang Fault, using helium isotopes and ratios of ^{20}Ne to ^{4}He, as the valley appears to represent a crustal-scale suture that separates the colliding arc and continent. We collected groundwater, hot spring, and bedrock samples along the valley and the surface trace of recognized faults. The aim was to identify helium anomalies and compare areas that appear to be creeping aseismically with areas that appear inactive or moved during recent seismic events. This study wants to clarify the importance of active faults with a well-defined and relatively simple geometry as conduits for mantle-derived fluids that can be traced to lower crust or mantle depths in the plate boundary suture.

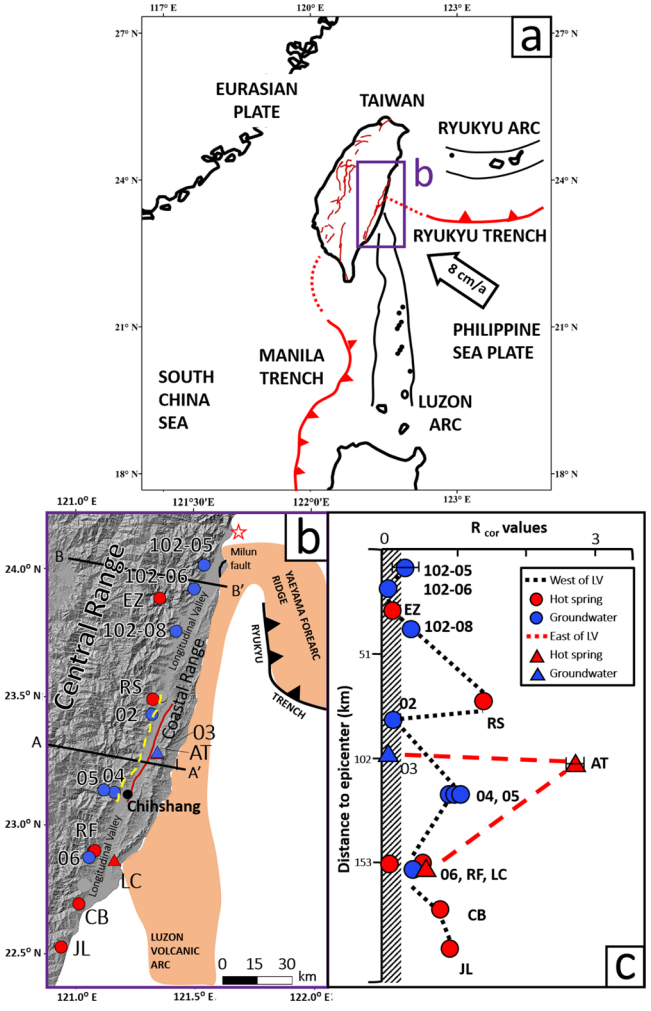

Figure 1. (a) Plate tectonic setting of Taiwan and its vicinity, showing the interaction of the Philippine Sea and Eurasian Plates and development of Ryukyu and Luzon arc systems (revised from Chen et al.[8]). (b) Tectonostratigraphic units of eastern Taiwan and sample locations. The major units (from west to east), including the Coastal Range, LV, and Central Range, with the red line representing the Chihshang Fault and the yellow dashed line representing the Central Range Fault. The orange area marks the volcanic arc. Epicenter of the 2018 M_w 6.4 Hualien earthquake (red star) is shown for reference. Water samples were collected from hot springs (solid red circles: from the west of LV; solid red triangles: from the east of LV), groundwater in well (solid red circles: from the west of LV; solid red circles: from the east of LV), and rock samples were from well cores (wells 102-08, 02, 03, 04, and 05). (c) Distribution of R_{cor} value of samples collected before the earthquake is plotted based on the geographic positions projected from (b), in which the R/R_A values of rock samples construct the slash-shaded bar.

2. TECTONIC AND GEOLOGIC SETTINGS

The Taiwan orogenic belt is located at the convergent boundary between the Eurasian Plate and Philippine Sea Plate, although the boundary has a relatively unusual geometry (Figure 1a).[25,28−30] In the south, the continental margin of Eurasia is subducting southeast beneath the Philippine Sea Plate; whereas in the north, the Philippine Sea Plate itself is subducting beneath Eurasia; that is, the subduction zone reverses polarity from south to north. In addition, the progressive subduction of the continental crust along the southern boundary results in the possible subduction of the forearc, the growth of the Taiwan accretionary wedge, and the development of a collision-related suture between the orogenic belt and the colliding magmatic arc on the Philippine Sea Plate. The LV marks the surface trace of this arc-accretionary wedge suture.

Geologically, the suture is marked, in part, by outcrops of serpentinized mafic and ultramafic rocks in the eastern Central Range (i.e., the Yuli metamorphic belt) and blocks of mafic rocks representing a disrupted ophiolite in the western Coastal Range (i.e., the Lichi Mélange).[21,31] The mafic blocks of the Yuli belt record high pressure metamorphism and are interpreted to represent the deeper levels of an accretionary wedge that formed during subduction of the South China Sea oceanic crust in the middle-late Miocene.[32−34] Subsequently, rapid uplift of the metamorphic belt was probably driven by extrusion as the continental crust was subducted in Pliocene arc−continent collision. The blocks of mafic rocks in the Lichi Mélange include gabbro, peridotite, red shale, and an extrusive tholeiitic sequence including glassy pillow lavas and are intercalated with early-Pliocene coherent forearc sediments.[22,31] The mafic rocks in both units with mantle affinities are ∼15 Ma and may represent fragments of the same piece of oceanic crust.

The suture is also marked by a complex system of active or recently active faults, including the Chihshang Fault mentioned above and the Milun Fault in Hualien City, which generally trace the break in the slope along the east and west sides of the LV. The Milun Fault forms the western boundary of a small terrace in Hualien City and was reactivated as a high-angle reverse fault during the M_w 6.4 Hualien earthquake on February 6, 2018 (the 2018 Hualien earthquake).[35] The fault slipped 0.8 m left laterally and 16 cm vertically during the earthquake causing extensive damage to the infrastructure along the fault trace. Seventeen inhabitants were killed and over 295 people were injured by collapsed buildings and subsequent landslides. The Milun Fault appears, in part, to be a northeast-dipping, high-angle reverse fault, but estimates of the geometry of the fault that slipped during the earthquake suggest a more westerly dip beneath the Central Range.[36]

South of the Milun fault but in the northern end of the LV, Chuang et al.[37] identified a west-dipping blind reverse fault

https://dx.doi.org/10.1021/acsearthspacechem.0c00038
ACS Earth Space Chem. 2020, 4, 1237−1246

Table 1. Sampling Site, Depth, and $^3He/^4He$ and $^{20}Ne/^4He$ Ratios of Hot Spring Samples in Eastern Taiwan[b]

sample name	latitude	longitude	altitude (m)	depth (m)	water temperature (°C)	^4He[a] (cm^3 STP/g)	^{20}Ne[a] (cm^3 STP/g)	$^3He/^4He$[c] (R/R_A)	$^{20}Ne/^4He$[c]	r	R_{cor}[c]
EZ	121.36	23.88	654	outcrop	50	4.43×10^{-6}	4.65×10^{-6}	0.41 ± 0.01	0.95 ± 0.10	0.32	0.14 ± 0.04
RS	121.36	23.50	130	500	50.4	2.41×10^{-7}	3.63×10^{-8}	1.33 ± 0.02	0.15 ± 0.01	0.05	1.35 ± 0.02
AT	121.34	23.28	182	outcrop	62.9	4.17×10^{-6}	6.71×10^{-6}	2.14 ± 0.15	0.62 ± 0.06	0.20	2.68 ± 0.22
LC	121.16	22.86	236	outcrop	33.5	8.98×10^{-7}	2.19×10^{-6}	0.87 ± 0.02	0.41 ± 0.04	0.69	0.58 ± 0.12
RF-1	121.07	22.90	184	outcrop	54.5	6.82×10^{-7}	2.25×10^{-7}	0.63 ± 0.02	0.33 ± 0.12	0.11	0.59 ± 0.02
RF-2	121.08	22.90	186	>200	64.7	2.38×10^{-7}	2.70×10^{-7}	0.45 ± 0.02	1.14 ± 0.002	0.42	0.05 ± 0.02
CB	121.02	22.69	81	unknown	49.2	1.95×10^{-6}	1.09×10^{-6}	0.93 ± 0.06	1.83 ± 0.18	0.55	0.84 ± 0.06
JL	120.94	22.53	50	115	94.3	6.27×10^{-8}	7.51×10^{-8}	0.99 ± 0.02	1.20 ± 0.002	0.58	0.98 ± 0.02

[a]Reported uncertainties for ^4He and ^{20}Ne contents are estimated at ±6% (2σ). [b]Analytical uncertainties in a single measurement are <0.5% for Helix SFT and <2% for Micromass 5400. [c]Error is 2σ.

beneath the eastern Central Range based on GPS and strong-motion seismic data and proposed that it represented a back thrust in the orogenic wedge. A west-dipping structure in this area of the Central Range is consistent with the inferred geometry of the Milun Fault and with tectonic models of subduction reversal. Further south in the valley, several faults have been mapped on the surface but only the Chihshang Fault is well-defined at depth. The distribution of earthquakes, mainly aftershocks following the 2003 M_w = 6.8 Chungkung earthquake, and the modeling of GPS data show an east-dipping, listric fault that extends to ~25 km.[38,39] The fault has been studied in detail near Chihshang Village (Figure 1b) and is creeping aseismically at a relatively high slip rate of ~43 mm/yr.[26,40,41] Fu et al.[42] investigated the Chihshang Fault using soil gases and argued that changes in gas composition with time were related to creeping activity along the fault.

3. METHODS

3.1. Sampling Locations and Analyses. Eight hot spring samples were collected in 50 mL lead glass bottles with two-end cocks under high vacuum, and 17 groundwater samples were collected with 15 cm^3 copper tubes from different sites on the both sides of the LV (Figure 1). Hot spring samples were collected from nationally recognized scenic spots where hot water flows from either natural outcrops or drilled wells. These waters are generally hotter than shallow groundwater and therefore may represent a deeper source. Two of the wells also yielded relatively hot water (e.g., 35.5 °C at sites 04-S and 04-D). Ten of the groundwater samples were collected two to five years before the 2018 Hualien Earthquake (Figure 1b; Table 2) and seven well samples were collected after the earthquake (13th February, 2018). The wells sampled after the earthquake ranged from 21 to 126 km from the epicenter. After sampling, all containers were sealed with steel clamps to eliminate possible exchange with atmospheric helium.[15]

Dissolved gases were carefully extracted from the water sample and introduced into an all-metal vacuum system.[15] Helium and neon were purified in activated-charcoal traps with titanium getters at liquid nitrogen temperature.[43] The $^4He/^{20}Ne$ ratio was determined on a quadrupole mass spectrometer, Pfeiffer QMS 100, at the Atmosphere Ocean Research Institute (AORI), University of Tokyo, with a 2σ of ±6%.[43] After separating from neon using a cryogenic charcoal trap at 40 K, helium was introduced into a isotope mass spectrometer, GV INSTRUMENT Helix SFT, for $^3He/^4He$ analysis.[44,45] Replicate measurements made on a Japan helium standard (Helium standard of Japan) show a reproducibility of ±0.03% (2 RSD).[44] $^3He/^4He$ and $^{20}Ne/^4He$ ratios of hot spring samples of EZ, AT, LC, and CB were measured with the Micromass 5400 noble gas mass spectrometer in the Department of Geosciences, National Taiwan University. Details of the measurements have been given by Yang[46] and Yang et al.[47] Air was routinely run as a standard for calibration. A pure helium gas standard of the helium standard of Japan was also prepared as the working standard to reduce the analytical errors. The overall 2σ errors on isotopic ratios are ±2−7%.[48] Isotopic errors in this study are all two standard deviations unless otherwise noted.

Five 100 g samples of metasandstones and fine-grained shale were also collected from drilled well cores at depths ranging from 90 to 100 m (Table 3). The rock samples were subsampled into 0.25 g sizes that were washed in an ultrasonic bath of distilled water, dried, and wrapped in Al foil. The samples were then loaded into a glass sample holder that was attached to the top of double-walled tantalum crucible that included a resistivity heater. Prior to running step-heating experiments, the samples were heated to 150 °C and evacuated overnight using a turbo molecular pump to ensure that all volatiles inside the crusher and on the surface of samples pumped out. The samples were then stepwise heated to 1800 °C for gas extraction. The thallium furnace containing the samples was directly connected to the purification line under vacuum and the extracted gases were directly introduced into an all-metal vacuum system.[49]

3.2. Correction of Atmospheric Helium Contamination. Helium isotope composition in water samples can be altered by air originally trapped inside the groundwater reservoir. The $^3He/^4He$ ratio for diminishing air contribution should be corrected with the observed $^4He/^{20}Ne$ ratio by the following formula[8,9,15,50,51]

$$R_{cor} = [(^3He/^4He)_{meas} - r]/(1 - r)$$

$$r = (^4He/^{20}Ne)_{ASW}/(^4He/^{20}Ne)_{meas}$$

where R_{cor} and $(^3He/^4He)_{meas}$ denote the corrected and measured $^3He/^4He$ ratios, respectively, $(^4He/^{20}Ne)_{ASW}$ is the $^4He/^{20}Ne$ ratio of the ASW, and $(^4He/^{20}Ne)_{meas}$ is the observed $^4He/^{20}Ne$ ratio of the sample. The $(^4He/^{20}Ne)_{ASW}$ ratio was calculated using the solubility formula ($^4He/^{20}Ne$ = 0.249 at 10 °C) and sampling temperature.[52,53] The propagated uncertainty of calculated R_{cor} can be aggravated with large analytical errors of isotopic ratios. For example, analytical errors of $(^3He/^4He)_{meas}$ for samples of EZ, AT, LC, and CB, measured on Micromass 5400, are ±2−7% and the induced errors for R_{cor} values are ±7−28%. Detailed uncertainty calculation was described in Sano et al.[15]

https://dx.doi.org/10.1021/acsearthspacechem.0c00038
ACS Earth Space Chem. 2020, 4, 1237−1246

Table 2. Sampling Site, Depth, and $^3He/^4He$ and $^{20}Ne/^4He$ Ratios of Groundwater Samples before and after the 2018 M_w 6.4 Hualien Earthquake

sample name	latitude	longitude	altitude (m)	depth (m)	water temperature (°C)	distance[a] (km)	^4He[b] (cm^3STP/g)	^{20}Ne[b] (cm^3STP/g)	$^3He/^4He$[c] (R/R_A)	$^{20}Ne/^4He$[c]	r	R_{cor}[c]
Before EQ												
102-05	121.54	24.01	125	100	24.6	20.779	5.36×10^{-8}	1.56×10^{-7}	0.86 ± 0.02	2.91 ± 0.02	0.80	0.49 ± 0.34
102-06	121.50	23.92	160	100	22.8	31.348	1.67×10^{-7}	1.98×10^{-7}	0.41 ± 0.02	1.19 ± 0.02	0.32	0.16 ± 0.02
102-08	121.42	23.76	174	100	25.2	50.797	1.06×10^{-7}	2.61×10^{-7}	0.79 ± 0.02	2.46 ± 0.02	0.67	0.46 ± 0.14
02	120.72	23.13	160	100	24.8	87.377	1.24×10^{-7}	2.49×10^{-7}	0.62 ± 0.02	2.01 ± 0.001	0.55	0.24 ± 0.06
03	120.60	22.93	259	35	25.8	101.364	1.09×10^{-7}	1.43×10^{-7}	0.42 ± 0.02	1.32 ± 0.001	0.36	0.14 ± 0.02
04S	120.68	22.90	342	38	35.5	124.743	6.55×10^{-7}	2.10×10^{-7}	0.82 ± 0.02	0.32 ± 0.02	0.11	0.80 ± 0.02
04D	120.68	22.90	342	100	35.5	124.743	5.58×10^{-7}	2.11×10^{-7}	1.12 ± 0.02	0.38 ± 0.01	0.09	1.13 ± 0.02
05	120.67	22.71	418	100	29.6	125.886	1.49×10^{-6}	1.74×10^{-7}	0.80 ± 0.02	0.12 ± 0.01	0.03	0.79 ± 0.02
06	120.66	22.53	240	100	30.3		9.74×10^{-8}	2.32×10^{-7}	0.81 ± 0.02	2.38 ± 0.001	0.66	0.53 ± 0.12
01	121.04	22.76	154	100	26.2		1.06×10^{-7}	2.44×10^{-7}	0.65 ± 0.01	2.07 ± 0.02	0.57	0.18 ± 0.02
After EQ												
102-05	121.54	24.01	125	100	18.8	20.779	4.43×10^{-8}	1.70×10^{-7}	0.98 ± 0.02	3.85 ± 0.0002	1.03	0.52 ± 0.24
102-06	121.50	23.92	160	100	21.4	31.348	4.64×10^{-8}	1.81×10^{-7}	0.97 ± 0.02	3.90 ± 0.001	1.04	0.31 ± 0.24
102-08	121.42	23.76	174	100	26	50.797	5.24×10^{-8}	1.97×10^{-7}	0.99 ± 0.02	3.77 ± 0.001	1.02	0.84 ± 0.18
02	120.72	23.13	160	100	22	87.377	6.00×10^{-8}	1.94×10^{-7}	0.85 ± 0.02	3.23 ± 0.001	0.86	0.23 ± 0.68
03	120.60	22.93	259	100	18.3	101.364	1.04×10^{-7}	1.78×10^{-7}	0.50 ± 0.02	1.70 ± 0.001	0.46	0.13 ± 0.02
04D	120.68	22.90	342	100	20	124.743	1.49×10^{-7}	1.81×10^{-7}	0.87 ± 0.02	1.60 ± 0.004	0.33	0.78 ± 0.02
05	120.67	22.71	418	100	20.6	125.886	2.41×10^{-7}	1.49×10^{-7}	0.73 ± 0.02	0.62 ± 0.004	0.17	0.68 ± 0.02

[a]Distance is calculated from the epicenter of the 0206 Hualien earthquake. [b]Reported uncertainties for ^4He and ^{20}Ne contents are estimated at ±6% (2σ). Analytical uncertainties in a single measurement are <0.5%. [c]Error is 2σ.

https://dx.doi.org/10.1021/acsearthspacechem.0c00038
ACS Earth Space Chem. 2020, 4, 1237−1246

Table 3. Helium Contents and Isotopic Ratios of Rock Samples Possibly Composed in the Aquifer System in the Eastern Taiwan

Sample name	latitude	longitude	lithology	depth (m)	He content (cm^3STP/g)	$^3He/^4He^a$ (R/R_A)
102-08	121.42	23.76	slate	100	5.0×10^{-10}	0.03 ± 0.02
106-02	120.72	23.13	shist/phyllite	100	9.0×10^{-10}	0.25 ± 0.16
106-03	120.60	22.93	alternations of sandstone & shale	100	4.0×10^{-10}	0.03 ± 0.01
106-04	120.68	22.90	shist/phyllite	100	3.5×10^{-9}	0.25 ± 0.10
106-05	120.67	22.71	shist	100	6.7×10^{-9}	0.19 ± 0.10

[a]Error is 2σ.

4. GEOCHEMICAL RESULTS

4.1. Helium Isotopes of Groundwater Samples. All ^4He and ^{20}Ne concentrations and ratios and $^3He/^4He$ ratios of hot spring and groundwater samples and those of rock samples are listed in Tables 1−3 and plotted in Figure 2. Water-

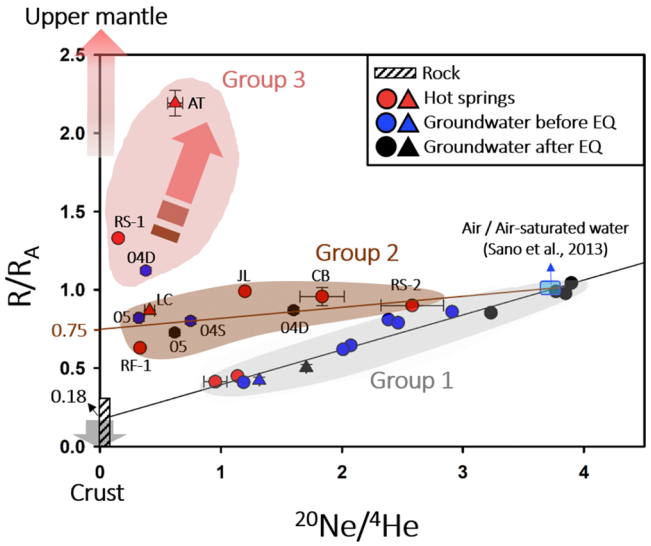

Figure 2. Correlation between the helium isotopic ratio (R/R_A) and $^{20}Ne/^4He$ ratio (with 2σ error bars) for hot spring (red) and groundwater (blue and black) samples before and after the 2018 M_w 6.4 Hualien earthquake, respectively. Bedrock samples: black and white stripe, and the range of their R/R_A value is 0.03−0.25 ± 0.22 (with 2σ error bars). Symbols of water samples correlate with Figures 1c and 3. The lines show proposed mixing curves of three end-member components: upper mantle, crust, and air/air saturated water with the vertical axis showing the contribution of $^3He/^4He$ from the crust or upper mantle. Group 1, 2, and 3 mark samples with different degrees of the mantle input.

dissolved ^4He contents range from 8.4×10^{-8} to 4.4×10^{-6} cm^3/g for hot spring and from 4.4×10^{-8} to 1.5×10^{-6} cm^3/g for ground water at respective sampling temperatures of 33.5−99.4 and 18.3−35.5 °C at 1 atm. $^3He/^4He$ ratios (R/R_A), normalized to an atmospheric ratio[6] (R_A) of 1.382×10^{-6}, vary significantly from 0.41 to 2.14 R/R_A of hot spring samples and 0.41 to 1.12 R/R_A of groundwater samples. R_{cor} values of hot spring and groundwater samples are in the range of 0.05−2.68 R/R_A and 0.13−1.13 R/R_A, respectively. Dissolved ^{20}Ne of all water samples range from 3.6×10^{-8} to 2.7×10^{-7} cm^3/g. $^{20}Ne/^4He$ ratios of water samples vary from 0.00 to 0.90.

4.2. Helium Isotopes of Rock Samples. The five rock samples of metasandstone and fine-grained shale considered to represent the aquifer rock system for groundwater were also analyzed (Table 3). ^4He contents vary from 1.48×10^{-8} to 3.74×10^{-7} cm^3 per gram and show a R/R_A range of 0.03−0.25 and low $^{20}Ne/^4He$ ratios <0.57. The averaged He abundance is $(1.76 \pm 2.08) \times 10^{-7}$ cm^3 STP/g. The large uncertainties are because of sample 102-08 and 106-03 having 10 times higher ^4He contents and 10 times lower $^3He/^4He$ ratios than the other three samples.

5. DISCUSSION

5.1. Sources for Noble Gas Anomalies. Helium and neon, being inert, are excellent natural tracers to see through complex chemical processes that could affect other more reactive species.[54] Helium isotopic composition is further used to characterize mantle, crustal, and atmospheric sources. Generally, the $^3He/^4He$ ratio of the sample (R) is normalized to the $^3He/^4He$ ratio in air (R_A). Three possible sources have been differentiated in the geodynamical system, primordial helium (^3He, which originates from the continental or oceanic upper mantle/MORB), radiogenic helium (^4He, continuously produced by the decay of uranium and thorium-series elements in continental or oceanic crust), and helium in air or air-saturated water (ASW).[35] These sources are identified based on the following ratios: upper mantle with R/R_A = 6−8 R_A, $^{20}Ne/^4He \ll 0.01$; radiogenic with $R/R_A \approx 0.02$ R_A, $^{20}Ne/^4He \ll 0.01$; and ASW with $R/R_A \approx 1$ R_A, $^{20}Ne/^4He \approx 0.268$ based on temperature.[20]

Figure 2 shows the isotopic distribution of groundwater and hot spring data from along the LV, including results from before and after the 2018 M_w 6.4 Hualien earthquake. Most of the data fall between values for air and crust, except samples from sites AT, RS-1, and 04D that define Group 3. The remaining samples appear to form two mixing lines which intercept the R/R_A axis at values of 0.18 for Group 1 and 0.75 for Group 2. The intercept of 0.18 R_A of Group 1 is consistent with the mean R/R_A value of 0.17 ± 0.12 for the bedrock samples and confirms the dominant occurrence of crustal helium in these samples. The samples are therefore considered as "background sites." The intercept of 0.18 R_A, however, is three times higher than R/R_A ratios from background sites of western Central Range,[8] suggesting that the mafic rocks from either the Yuli Belt or the Lichi Mélange have diffused helium with high R/R_A ratios of helium that contaminated the local crustal signal. Alternatively, these sites may record relatively minor contamination by primordial helium. Group 2 of the samples defines a second mixing line that intercepts the y-axis at 0.75 R_A, which is about four times higher than values from the "crustal" mixing line (the black line of Group 1). This value is essentially identical to the helium isotopic signature obtained from the Chaochou Fault along the western Central Range (0.78 R_A[8]). Chen et al.[8] interpreted this higher value as the primordial ^3He leaking through an active fault of the sites in the western Central Range. Even though it is possible to imply

https://dx.doi.org/10.1021/acsearthspacechem.0c00038
ACS Earth Space Chem. 2020, 4, 1237−1246

a contemporary flux of the primordial ^{3}He leaking through along the LV, there are other candidates for the mantle helium source. Because the mafic rocks are ~15 Ma old and many inactive fault systems are recognized here, the value of 0.75 R_A here may be a combined consequence of mantle helium stored in past active faults (e.g., the Central Range Fault) and derived from products of past volcanism stored in the region. Finally, Group 3 suggests a significant addition of mantle-derived ^{3}He in these samples because they have elevated R/R_A ratios compared to the two air/ASW-crust groups.

Water samples of Group 3 (Figure 2) have elevated helium isotopic signatures and correlate with the lateral extent of the Central Range and Chihshang Faults, suggesting that either or both of the faults may have acted as a significant conduit for mantle helium.[3] The absence of active volcanism along the valley supports this interpretation. Although samples AT and 03 overlap geographically, their He isotopic ratios are strongly different. This discrepancy of values might be because of the different conduits. Sample AT is from a natural hot spring, which may be representative of fluid sources at depth, coming from high temperatures in a region with excess heat flow. On the other hand, sample 03 is from a relatively shallow aquifer (<100 m depth) with lower temperature, which might include obvious signature derived from ASW/air. Samples from nonvolcanic areas with an elevated R/R_A ratio in previous studies have also been used in combination with the spatial correlation with faults to argue for fluid fluxes from the mantle.[14,20,55−57] In these studies, the influx of mantle fluids with high R/R_A ratios are interpreted as helium exsolving from partially melted zones in the upper mantle that subsequently traverse the entire crust via a permeable crustal-scale fault zone.[54] In Taiwan, a difference in seismicity may provide an explanation for the difference of the mantle input in the northern and southern ends of the valley. The actively creeping Chihshang Fault provides a likely conduit for mantle fluids in this area of the LV, as seismic data and modeling suggest that it is deeply rooted beneath the arc.

5.2. Temporal Variations Related to the 2018 M_w 6.4 Hualien Earthquake. The 2018 Hualien earthquake undoubtedly caused significant deformation and volume changes that may have released helium from the country rock or motivated fluid flow in the surrounding rocks. This degassed helium, either radiogenic ^{4}He from bedrock or primordial ^{3}He from volcanic minerals, may change the distribution of helium isotopes in fluids as they migrate through the rocks or fault zones. To aid in evaluating these possible effects on isotopic values collected from well water,[19,20] we show the values of different isotopes and their ratios relative to the distance from the earthquake epicenter, both before and after the earthquake (Figure 3). Isotopic values and ratios include ^{4}He and ^{20}Ne contents, ^{3}He/^{4}He ratios (R/R_A), and r and R_{cor} values.

Relative to the distance from the epicenter, the values of r show the clearest trends before and after the earthquake (Figure 3d). Values of r can range from 0 to 1 and represent the percentage of air detected in the samples from 0 to 100%. Before the earthquake and near the epicenter, values of r range [illegible] and decrease systematically to near 0.0 at 130 km from the epicenter. This pattern of decreasing r away from [illegible] appears to be enhanced after the earthquake, with postearthquake values ranging from ~1.0 near the epicenter to ~0.2 at 130 km from the epicenter. Both patterns are therefore consistent with an increase in atmospheric

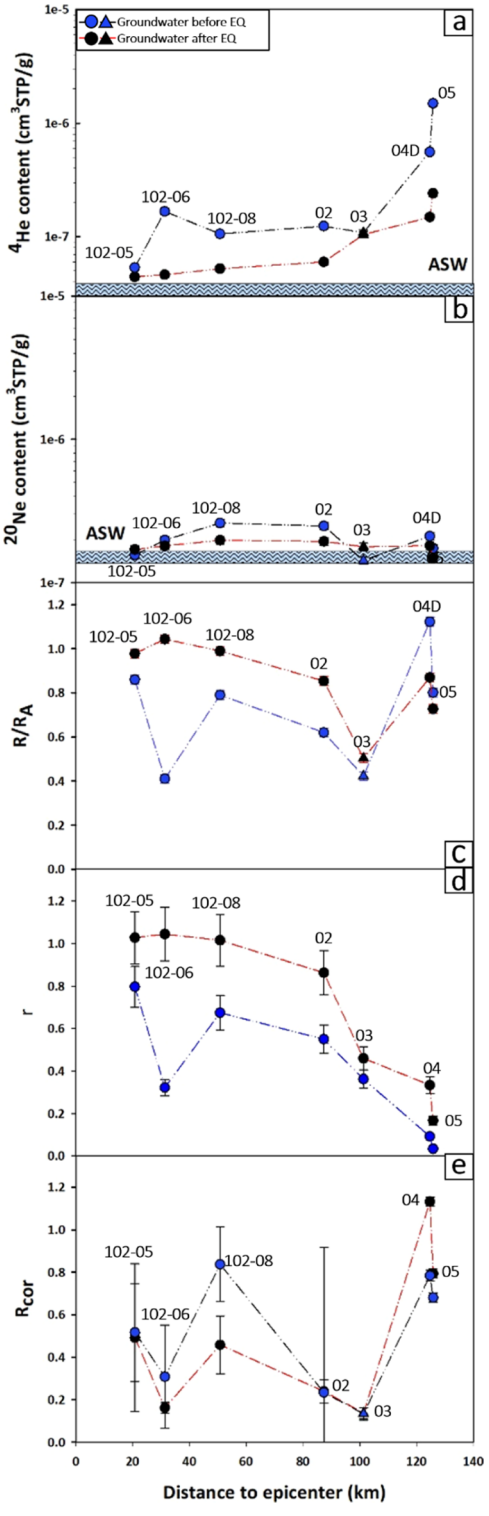

Figure 3. Graphs showing relation between noble gas content, or their ratios normalized to air/ASW, relative to the distance along the LV from the epicenter of the 2018 M_w 6.4 Hualien earthquake. (a) ^{4}He content, (b) ^{20}Ne content, (c) R/R_A the ratio of dissolved helium in the samples. (d) r the percentage of air detected in the samples and (e) R_{cor} the corrected R/R_A value for atmospheric helium. ASW denotes the value of air-saturated water. Note that all noble gas contents in the samples are higher than those in ASW as air pressures are higher beneath the surface. The general increase in ^{4}He away from the epicenter and the decrease after the earthquake.

https://dx.doi.org/10.1021/acsearthspacechem.0c00038
ACS Earth Space Chem. 2020, 4, 1237−1246

contributions near the epicenter and after the earthquake. This pattern is also suggested by the ^{4}He content which shows a slight increase away from the epicenter and a consistent decrease at all sites after the earthquake (Figure 3a). R/R_A data are also consistent with the r and ^{4}He results except at the site farthest from the epicenter where there the values overlap (Figure 3a,c,d). Finally, the changes in ^{20}Ne and R_{cor} (Figure 3b,e) are less conclusive.

In evaluating the effect of rainfall and an influx of groundwater on the measured isotopic values, we note that the 2018 Hualien earthquake occurred in February, which is the middle of the dry season in Taiwan, whereas sampling prior to the earthquake occurred in June and July, the middle of the summer monsoons in Taiwan (Central Weather Bureau of Taiwan, https://www.cwb.gov.tw/V8/C/D/DailyPrecipitation.html). This general pattern of seasonal rains is also consistent with the rainfall totals for the months prior to and just after the earthquake. For example, the total rainfall for the month of June 2013 (for sites 102-5, 102-06, and 102-8) was 175.5 mm and for July 2017 (for sites 02, 03, 04, and 05), it was 215.8 mm. In contrast, the total rainfall for January 2018, before the earthquake, was 96.0 mm for the sites sampled in 2013 and 53.9 mm for the sites sampled in 2017. We infer, therefore, that the rocks in the subsurface were relatively dry during the earthquake and that any mantle signal would be less diluted than if the samples had been collected during the wet season.

A volumetric strain change of rocks due to an earthquake could induce the helium isotopic change.[19] In this study, however, the ^{4}He contents released from rocks with a uranium content of 0.46−1.58 ppm could not be calculated because of the decrease of solubility of HeA.[58] Taken together, the isotopic data and ratios argue for more atmospheric contamination near the earthquake epicenter both before and after the earthquake. That is, the earthquake seems to have enhanced the degree of atmospheric mixing observed before the earthquake. Comparing the trends recognized in Taiwan with similar studies along the San Andreas Fault system in California,[55] the North Anatolian Fault zone in Turkey,[56] the Karaforam fault in Tibet, and the Futagawa−Hinagu fault,[14,20] the location-dependent variations of R/R_A and r values before and after the Hualien earthquake (Figure 3b) support the hypothesis that noble gas signatures are affected by an earthquake. In the case of eastern Taiwan, however, the earthquake apparently did not change the flow from the mantle according to the helium data of this study. Interestingly, the highest contribution of mantle fluids appears to be near the Chihshang Fault, although this relatively strong signal was not detected by the well data.

5.3. Connection of He-Isotope Data to Tectonic Features. Two regional-scale schematic cross sections adapted from Huang et al.[59] provide important context for our interpretation of the distribution of the mantle-derived fluids sampled along the LV (Figure 4). In the south, between Rueisuei and Chihshang (about 23°10′ N), the subducting plate and plate boundary dip in same direction (east) and generating relatively simple structural geometries. Further north, the subducting crust of Eurasia dips more steeply and the Philippine Sea Plate is starting to subduct and colliding with the continental crust of Eurasia and forming more complicated structural geometries. This fundamental change in plate geometries from south to north and the resulting changes in fault geometries, permeabilities,

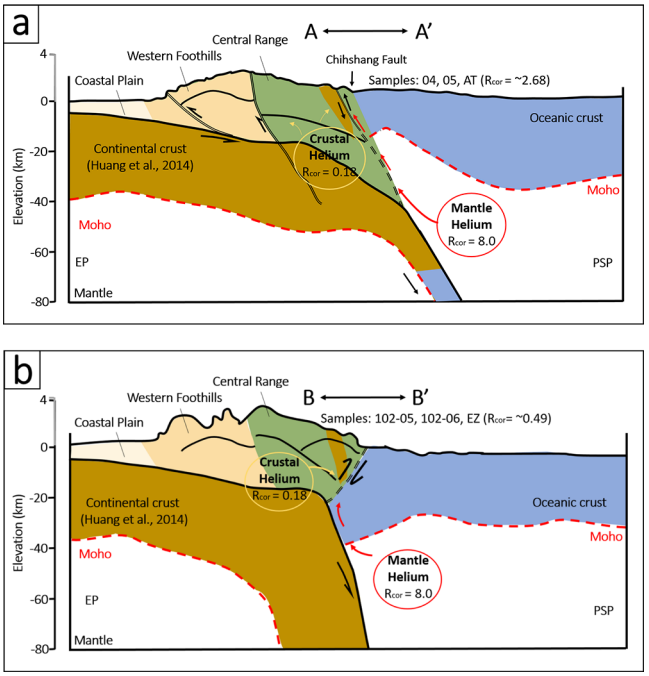

Figure 4. Schematic profiles across line A−A′ and B−B′ in Figure 1 (based on seismic tomography interpretation in Huang et al.[59]). Black double dashed lines indicate the Chihshang Fault and Central Range Fault. (a) As the Luzon volcanic arc approaches the Central Range, an east-dipping thrust fault appears, allowing the forearc oceanic lithosphere to also subduct underneath the volcanic arc lithosphere. Mantle helium migrates through these structures to the surface, where the highest R_A value in hot spring sample AT and groundwater samples 04 and 05 is observed. (b) North of the ~24.5° N latitude, the PSP-western edge seems to start dipping to the west to contact with the Eurasian lithosphere. Here, we observed the lower helium anomalies in 102-05, 102-06, and EZ than in AT.

and fluid flow patterns provide important context for interpreting the geochemical data. For example, the Chihshang Fault in the south is active and associated earthquakes define a relatively simple, listric geometry beneath the Luzon Arc, and the largest R_{cor} values occur at site AT in the middle of the mapped trace of the fault. R_{cor} values decrease to the north (RS) and south (04, 05) (Figure 1c; Figure 4a), although the values in these nearby sites are still more elevated than R_{cor} values to the north. Future research, particularly of hot spring samples, may help delineate the distribution of mantle contamination in this area. In the north, mapping and earthquake focal mechanisms suggest a more complicated fault system, and suggestions of mantle contamination are substantially weaker (sites 102-05, 102-06, and EZ) (Figure 4b). This change is also consistent with Moho geometries based on V_p and V_s seismic tomography and the distribution of moderate and deep earthquakes.[60,61]

Overall, these results complement the work by Chen et al.[8] who showed that mantle-derived fluids can penetrate the crust along fault-related conduits in a nonvolcanic arc−continent collision (see the fault system between Central Range and Western Foothills in Figure 4a). The conduit correlated with a deflection in the subducting continental crust and was identified, in part, through the distribution of nonvolcanic tremor and a zone of unusually high conductivity in the upper crust. However, in this study, we found the highest concentration of mantle helium directly above the most active

https://dx.doi.org/10.1021/acsearthspacechem.0c00038
ACS Earth Space Chem. 2020, 4, 1237−1246

structure associated the plate boundary suture, the Chihshang Fault. North of this relatively simple plate interface, the subduction direction flips (Figure 4) and mantle contamination appears to decrease. This change could be related to changes in fault permeability and tortuosity along the plate boundary faults in this area.

6. CONCLUSIONS

We conducted a regional study of noble gas isotopic compositions and contents of thermal fluids collected from bedrock samples, hot springs, and wells along the LV, eastern Taiwan, which represents the suture of the arc−continent collision. The results show that the highest mantle helium signatures are from a hot spring sample collected directly above the trace of the Chihshang Fault. This fault crops out along the east-central part of the valley and represents one of the most active structures along the suture zone. Although the high value comes from only one sample, the implication that the Chihshang Fault may serve as conduit for deep-sourced fluids is consistent with the geophysical data that show a well-developed fault zone extending to the lower crust. Additional data along and across strike will better define the distribution of the helium anomaly. Furthermore, seven groundwater samples were duplicated after the 2018 M_w 6.4 Hualien earthquake in the northern end of the valley to evaluate the influence of the seismic activity on the conductivity and evolution of the plate boundary suture in this area. The earthquake appears to be associated with a dilution of mantle-derived fluids in this area of the suture. At a regional-scale, our findings suggest that the flipping of the subduction polarity and the resulting increase in tortuosity in fluid flow paths may control the extent to which mantle noble gases reach the surface.

AUTHOR INFORMATION

Corresponding Authors

Timothy B. Byrne − *Department of Geosciences, University of Connecticut, Storrs, Connecticut 06269-1045, United States*; Email: tim.byrne@uconn.edu

Chuan-Chou Shen − *High-Precision Mass Spectrometry and Environment Change Laboratory (HISPEC), Department of Geosciences, Research Center for Future Earth, and Global Change Research Center, National Taiwan University, Taipei 10617, Taiwan, R.O.C.*; orcid.org/0000-0003-2833-2771; Email: river@ntu.edu.tw

Authors

Ai-Ti Chen − *High-Precision Mass Spectrometry and Environment Change Laboratory (HISPEC), Department of Geosciences and Research Center for Future Earth, National Taiwan University, Taipei 10617, Taiwan, R.O.C.*

Yuji Sano − *Atmosphere and Ocean Research Institute, The University of Tokyo, Kashiwa, Chiba 277-8564, Japan*; orcid.org/0000-0002-3305-5644

Naoto Takahata − *Atmosphere and Ocean Research Institute, The University of Tokyo, Kashiwa, Chiba 277-8564, Japan*

[illegible] Yang − *Department of Geosciences, National Taiwan University, Taipei 10617, Taiwan, R.O.C.*

[illegible] − *Central Geological Survey, MOEA, Taipei 23568, Taiwan, R.O.C.*

Complete contact information is available at: https://pubs.acs.org/10.1021/acsearthspacechem.0c00038

Author Contributions

The manuscript was written through contributions of all authors. All authors have given approval to the final version of the manuscript.

Notes

The authors declare no competing financial interest.

ACKNOWLEDGMENTS

We gratefully acknowledge Dr. Cheng-Hong Chen and Dr. Tsung-Kwei Liu in National Taiwan University for the inspiring thoughts on this manuscript. We appreciate all Gas Geochemistry Laboratory members from the National Taiwan University, especially Dr. Tzu-Chen Shen; Dr. Chien-Chung Ke from the Sinotech Engineering Consultants, Taipei, Taiwan; and Mr. Yen-Tsu Lin from the Central Geological Survey, MOEA, Taiwan, for assisting in collecting samples. This study was supported by the Central Geological Survey, MOEA, Taiwan (B10112; 106-5226904000-01-01). This study was also partially supported by grants from the Science Vanguard Research Program of the Ministry of Science and Technology[62] (108-2119-M-002-012), the National Taiwan University (109L8926), the Higher Education Sprout Project of the Ministry of Education, Taiwan, ROC (108L901001), and the US National Science Foundation (to Byrne, EAR-1220453).

REFERENCES

(1) Dewey, J. F. Suture zone complexities: A review. *Tectonophysics* **1977**, *40*, 53−67.

(2) Chemenda, A. I.; Yang, R.-K.; Stephan, J.-F.; Konstantinovskaya, E. A.; Ivanov, G. M. New results from physical modelling of arc-continent collision in Taiwan: evolutionary model. *Tectonophysics* **2001**, *333*, 159−178.

(3) Kennedy, B. M.; van Soest, M. C. Flow of mantle fluids through the ductile lower crust: Helium isotope trends. *Science* **2007**, *318*, 1433−1436.

(4) Sano, Y.; Nakajima, J. Geographical distribution of He-3/He-4 ratios and seismic tomography in Japan. *Geochem. J.* **2008**, *42*, 51−60.

(5) Caracausi, A.; Sulli, A. Outgassing of Mantle Volatiles in Compressional Tectonic Regime Away From Volcanism: The Role of Continental Delamination. *Geochem., Geophys., Geosyst.* **2019**, *20*, 2007−2020.

(6) Sano, Y.; Marty, B.; Burnard, P. Noble Gases in the Atmosphere. In *The Noble Gases as Geochemical Tracers*; Burnard, P., Ed.; Springer Berlin Heidelberg: Berlin, Heidelberg, 2013; pp 17−31.

(7) Hoke, L.; Lamb, S.; Hilton, D. R.; Poreda, R. J. Southern limit of mantle-derived geothermal helium emissions in Tibet: implications for lithospheric structure. *Earth Planet. Sci. Lett.* **2000**, *180*, 297−308.

(8) Chen, A.-T.; Shen, C.-C.; Byrne, T. B.; Sano, Y.; Takahata, N.; Yang, T. F.; Wang, Y. Mantle fluids associated with crustal-scale faulting in a continental subduction setting, Taiwan. *Sci. Rep.* **2019**, *9*, 10805.

(9) Craig, H.; Lupton, J.; Horibe, Y. A mantle helium component in circum-Pacific volcanic gases: Hakone, the Marianas, and Mt. Lassen. *Terrestrial Rare Gases*; Springer, 1978; pp 3−16.

(10) Ballentine, C. J. GEOCHEMISTRY: Tiny Tracers Tell Tall Tales. *Science* **2002**, *296*, 1247−1248.

(11) Baubron, J.-C.; Rigo, A.; Toutain, J.-P. Soil gas profiles as a tool to characterise active tectonic areas: the Jaut Pass example (Pyrenees, France). *Earth Planet. Sci. Lett.* **2002**, *196*, 69−81.

(12) Bulashevitch, Y. P.; Aleynikov, A. L.; Bellavin, O. V.; Bugaylo, V. A.; Khalevin, N. I.; Shapiro, V. A.; Tavrin, I. F.; Vlokh, N. P.; Zubkov, A. V. Geodynamics of Urals. *Tectonophysics* **1976**, *35*, 15−26.

(13) Gao, R.; Lu, Z.; Klemperer, S. L.; Wang, H.; Dong, S.; Li, W.; Li, H. Crustal-scale duplexing beneath the Yarlung Zangbo suture in the western Himalaya. *Nat. Geosci.* **2016**, *9*, 555−560.

(14) Klemperer, S. L.; Kennedy, B. M.; Sastry, S. R.; Makovsky, Y.; Harinarayana, T.; Leech, M. L. Mantle fluids in the Karakoram fault: Helium isotope evidence. *Earth Planet. Sci. Lett.* **2013**, *366*, 59−70.
(15) Sano, Y.; Takahata, N.; Seno, T. Geographical distribution of He-3/He-4 ratios in the Chugoku District, Southwestern Japan. *Pure Appl. Geophys.* **2006**, *163*, 745−757.
(16) Umeda, K.; Ninomiya, A.; McCrank, G. F. High 3He emanations from the source regions of recent large earthquakes, central Japan. *Geochem., Geophys., Geosyst.* **2008**, *9*, Q12003.
(17) Italiano, F.; Martelli, M.; Martinelli, G.; Nuccio, P. M. Geochemical evidence of melt intrusions along lithospheric faults of the Southern Apennines, Italy: Geodynamic and seismogenic implications. *J. Geophys. Res.: Solid Earth* **2000**, *105*, 13569−13578.
(18) Caracausi, A.; Martelli, M.; Nuccio, P. M.; Paternoster, M.; Stuart, F. M. Active degassing of mantle-derived fluid: A geochemical study along the Vulture line, southern Apennines (Italy). *J. Volcanol. Geotherm. Res.* **2013**, *253*, 65−74.
(19) Buttitta, D.; Caracausi, A.; Chiaraluce, L.; Favara, R.; Gasparo Morticelli, M.; Sulli, A. Continental degassing of helium in an active tectonic setting (northern Italy): the role of seismicity. *Sci. Rep.* **2020**, *10*, 162.
(20) Sano, Y.; Takahata, N.; Kagoshima, T.; Shibata, T.; Onoue, T.; Zhao, D. Groundwater helium anomaly reflects strain change during the 2016 Kumamoto earthquake in Southwest Japan. *Sci. Rep.* **2016**, *6*, 37939.
(21) Chi, W.-C.; Chen, L.; Liu, C.-S.; Brookfield, M. Development of arc-continent collision melanges: Linking onshore geological and offshore geophysical observations of the Pliocene Lichi Melange, southern Taiwan and northern Luzon arc, western Pacific. *Tectonophysics* **2014**, *636*, 70−82.
(22) Page, B. M.; Suppe, J. The Pliocene Lichi Melange of Taiwan - Its Plate-Tectonic and Olistostromal Origin. *Am. J. Sci.* **1981**, *281*, 193−227.
(23) Chang, C.-P.; Angelier, J.; Huang, C.-Y. Origin and evolution of a melange: the active plate boundary and suture zone of the Longitudinal Valley, Taiwan. *Tectonophysics* **2000**, *325*, 43−62.
(24) Chang, C. P.; Angelier, J.; Huang, C. Y.; Liu, C. S. Structural evolution and significance of a melange in a collision belt: the Lichi Melange and the Taiwan arc-continent collision. *Geol. Mag.* **2001**, *138*, 633−651.
(25) Huang, C.-Y.; Yuan, P. B.; Tsao, S.-J. Temporal and spatial records of active arc-continent collision in Taiwan: A synthesis. *Geol. Soc. Am. Bull.* **2006**, *118*, 274−288.
(26) Huang, C.-Y.; Yuan, P. B.; Lin, C.-W.; Wang, T. K.; Chang, C.-P. Geodynamic processes of Taiwan arc-continent collision and comparison with analogs in Timor, Papua New Guinea, Urals and Corsica. *Tectonophysics* **2000**, *325*, 1−21.
(27) Liou, J. G.; Ernst, W. G. Oceanic Ridge Metamorphism of the East Taiwan Ophiolite. *Contrib. Mineral. Petrol.* **1979**, *68*, 335−348.
(28) Barrier, E.; Angelier, J. Active Collision in Eastern Taiwan - the Coastal Range. *Tectonophysics* **1986**, *125*, 39−72.
(29) Bowin, C.; Lu, R. S.; Lee, C.-S.; Schouten, H. Plate Convergence and Accretion in Taiwan-Luzon Region. *AAPG Bull.* **1978**, *62*, 1645−1672.
(30) Ho, C. S. A Synthesis of the Geologic Evolution of Taiwan. *Tectonophysics* **1986**, *125*, 1−16.
(31) Chen, W.-S.; Chung, S.-L.; Chou, H.-Y.; Zugeerbai, Z.; Shao, W.-Y.; Lee, Y.-H. A reinterpretation of the metamorphic Yuli belt: Evidence for a middle-late Miocene accretionary prism in eastern Taiwan. *Tectonics* 2017, *36*, 188−206.
(32) Beyssac, O.; Negro, F.; Simoes, M.; Chan, Y. C.; Chen, Y. G. [illegible]orphism in Taiwan: from oceanic subduction to arc-continent collision? *Terra Nova* **2008**, *20*, 118−125.
(33) [illegible]otis, I.; Tsai, C.-H.; Ernst, W. G.; Jahn, B.-M.; Iizuka, Y. New P-T constraints on the Tamayen glaucophane-bearing rocks, eastern Taiwan: Perple_X modelling results and geodynamic implications. *J. Metamorph. Geol.* **2017**, *35*, 35−54.
(34) Keyser, W.; Tsai, C.-H.; Iizuka, Y.; Oberhänsli, R.; Ernst, W. G. High-pressure metamorphism in the Chinshuichi area, Yuli belt, eastern Taiwan. *Tectonophysics* **2016**, *692*, 191−202.
(35) Huang, M.-H.; Huang, H.-H. The Complexity of the 2018 M-W 6.4 Hualien Earthquake in East Taiwan. *Geophys. Res. Lett.* **2018**, *45*, 13249−13257.
(36) Central Geological Survey. *Report of the 20180206 Hualien Earthquake and Geologic Survey*, 2018; Vol. *119*.
(37) Chuang, R. Y.; Johnson, K. M.; Kuo, Y.-T.; Wu, Y.-M.; Chang, C.-H.; Kuo, L.-C. Active back thrust in the eastern Taiwan suture revealed by the 2013 Rueisuei earthquake: Evidence for a doubly vergent orogenic wedge? *Geophys. Res. Lett.* **2014**, *41*, 3464−3470.
(38) Angelier, J.; Chu, H.-T.; Lee, J.-C.; Hu, J.-C. Active faulting and earthquake hazard: The case study of the Chihshang Fault, Taiwan. *J. Geodyn.* **2000**, *29*, 151−185.
(39) Lee, J.-C.; Angelier, J.; Chu, H.-T.; Hu, J.-C.; Jeng, F.-S. Continuous monitoring of an active fault in a plate suture zone: a creepmeter study of the Chihshang Fault, eastern Taiwan. *Tectonophysics* **2001**, *333*, 219−240.
(40) Ching, K.-E.; Rau, R.-J.; Johnson, K. M.; Lee, J.-C.; Hu, J.-C. Present-day kinematics of active mountain building in Taiwan from GPS observations during 1995-2005. *J. Geophys. Res.: Solid Earth* **2011**, *116*, B09405.
(41) Angelier, J.; Chu, H.-T.; Lee, J.-C. Shear concentration in a collision zone: Kinematics of the Chihshang Fault as revealed by outcrop-scale quantification of active faulting, Longitudinal Valley, eastern Taiwan. *Tectonophysics* **1997**, *274*, 117−143.
(42) Fu, C.-C.; Yang, T. F.; Walia, V.; Liu, T.-K.; Lin, S.-J.; Chen, C.-H.; Hou, C.-S. Variations of soil-gas composition around the active Chihshang Fault in a plate suture zone, eastern Taiwan. *Radiat. Meas.* **2009**, *44*, 940−944.
(43) Sano, Y.; Wakita, H. Precise Measurement of Helium-Isotopes in Terrestrial Gases. *Bull. Chem. Soc. Jpn.* **1988**, *61*, 1153−1157.
(44) Sano, Y.; Tokutake, T.; Takahata, N. Accurate measurement of atmospheric helium isotopes. *Anal. Sci.* **2008**, *24*, 521−525.
(45) Sano, Y.; Hara, T.; Takahata, N.; Kawagucci, S.; Honda, M.; Nishio, Y.; Tanikawa, W.; Hasegawa, A.; Hattori, K. Helium anomalies suggest a fluid pathway from mantle to trench during the 2011 Tohoku-Oki earthquake. *Nat. Commun.* **2014**, *5*, 3084.
(46) Yang, T. F. The helium isotopic ratios of fumaroles from Tatun Volcano Group of Yangmingshan National Park, N. Taiwan. *J. Natl. Park* **2000**, *10*, 73−94.
(47) Yang, T. F.; Lan, T. F.; Lee, H.-F.; Fu, C.-C.; Chuang, P.-C.; Lo, C.-H.; Chen, C.-H.; Chen, C.-T. A.; Lee, C.-S. Gas compositions and helium isotopic ratios of fluid samples around Kueishantao, NE offshore Taiwan and its tectonic implications. *Geochem. J.* **2005**, *39*, 469−480.
(48) Matsuda, J.; Matsumoto, T.; Sumino, H.; Nagao, K.; Yamamoto, J.; Miura, Y.; Kaneoka, I.; Takahata, N.; Sano, Y. The He-3/He-4 ratio of the new internal He Standard of Japan (HESJ). *Geochem. J.* **2002**, *36*, 191−195.
(49) Sano, Y.; Toyoda, K.; Wakita, H. He-3-He-4 Ratios of Marine Ferromanganese Nodules. *Nature* **1985**, *317*, 518−520.
(50) Horiguchi, K.; Ueki, S.; Sano, Y.; Takahata, N.; Hasegawa, A.; Igarashi, G. Geographical distribution of helium isotope ratios in northeastern Japan. *Isl. Arc* **2010**, *19*, 60−70.
(51) McCrory, P. A.; Constantz, J. E.; Hunt, A. G.; Blair, J. L. Helium as a tracer for fluids released from Juan de Fuca lithosphere beneath the Cascadia forearc. *Geochem., Geophys., Geosyst.* **2016**, *17*, 2434−2449.
(52) Ozima, M.; Podosek, F. A. *Noble Gas Geochemistry*; Cambridge University Press, 2002.
(53) Weiss, R. F. Solubility of Helium and Neon in Water and Seawater. *J. Chem. Eng. Data* **1971**, *16*, 235−241.
(54) Ballentine, C. J.; Sherwood Lollar, B. Regional groundwater focusing of nitrogen and noble gases into the Hugoton-Panhandle giant gas field, USA. *Geochim. Cosmochim. Acta* **2002**, *66*, 2483−2497.
(55) Kennedy, B. M.; Kharaka, Y. K.; Evans, W. C.; Ellwood, A.; DePaolo, D. J.; Thordsen, J.; Ambats, G.; Mariner, R. H. Mantle fluids

https://dx.doi.org/10.1021/acsearthspacechem.0c00038
ACS Earth Space Chem. 2020, 4, 1237−1246

in the San Andreas fault system, California. *Science* **1997**, *278*, 1278−1281.
(56) Dogan, T.; Sumino, H.; Nagao, K.; Notsu, K.; Tuncer, M. K.; Celik, C. Adjacent releases of mantle helium and soil CO2 from active faults: Observations from the Marmara region of the North Anatolian Fault zone, Turkey. *Geochem., Geophys., Geosyst.* **2009**, *10*, Q11009.
(57) Caracausi, A.; Favara, R.; Italiano, F.; Nuccio, P. M.; Paonita, A.; Rizzo, A. Active geodynamics of the central Mediterranean Sea: Tensional tectonic evidences in western Sicily from mantle-derived helium. *Geophys. Res. Lett.* **2005**, *32*, L04312.
(58) Jahn, B.-m. Pb-Pb Dating of Young Marbles from Taiwan. *Nature* **1988**, *332*, 429−432.
(59) Huang, H.-H.; Wu, Y.-M.; Song, X.; Chang, C.-H.; Lee, S.-J.; Chang, T.-M.; Hsieh, H.-H. Joint Vp and Vs tomography of Taiwan: Implications for subduction-collision orogeny. *Earth Planet. Sci. Lett.* **2014**, *392*, 177−191.
(60) Ustaszewski, K.; Wu, Y.-M.; Suppe, J.; Huang, H.-H.; Chang, C.-H.; Carena, S. Crust-mantle boundaries in the Taiwan-Luzon arc-continent collision system determined from local earthquake tomography and 1D models: Implications for the mode of subduction polarity reversal. *Tectonophysics* **2012**, *578*, 31−49.
(61) Hsu, Y.-J.; Yu, S.-B.; Simons, M.; Kuo, L.-C.; Chen, H.-Y. Interseismic crustal deformation in the Taiwan plate boundary zone revealed by GPS observations, seismicity, and earthquake focal mechanisms. *Tectonophysics* **2009**, *479*, 4−18.
(62) Clévédé, E.; Bukchin, B.; Favreau, P.; Mostinskiy, A.; Aoudia, A.; Panza, G. F. Long-period spectral features of the Sumatra-Andaman 2004 earthquake rupture process. *Geophys. J. Int.* **2012**, *191*, 1215−1225.

https://dx.doi.org/10.1021/acsearthspacechem.0c00038
ACS Earth Space Chem. 2020, 4, 1237−1246